SUPPORTING INFORMATION FOR THE ARTICLE:

Mechanisms for the Generation of Two Quadruplications Associated with Split-Hand Malformation

Shen Gu[1], Jennifer E. Posey[1], Bo Yuan[1], Claudia M.B. Carvalho[1], H.M. Luk[2], Kelly Erikson[3], Ivan F.M. Lo[2], Gordon K.C. Leung[5,6], Curtis R. Pickering[3], Brian H.Y. Chung[4,5] and James R. Lupski[1,6,7,8,*]

[1]Department of Molecular & Human Genetics, Baylor College of Medicine, Houston, TX 77030, USA.

[2]Clinical Genetic Service, Department of Health, Hong Kong, China

[3]Department of Head and Neck Surgery, The University of Texas MD Anderson Cancer Center, Houston, TX 77030, USA

[4]Department of Paediatrics and Adolescent Medicine, Queen Mary Hospital, Li Ka Shing Faculty of Medicine, The University of Hong Kong, Hong Kong, China

[5]Department of Obstetrics & Gynaecology, Li Ka Shing Faculty of Medicine, The University of Hong Kong, Hong Kong, China

[6]Department of Pediatrics, Baylor College of Medicine, Houston, TX 77030, USA.

[7]Human Genome Sequencing Center, Baylor College of Medicine, Houston, TX 77030, USA.

[8]Texas Children's Hospital, Houston, TX 77030, USA.

*** To whom correspondence should be addressed:**

James R. Lupski

Tel: 1-713-798-6530

Fax: 1-713-798-5073

E-mail: jlupski@bcm.edu

SUPP. MATERIALS AND METHODS

Subjects

This study was approved by the Institutional Review Board for Human Subject Research at BCM (IRB No. H-25466). Informed consent was obtained.

High-density aCGH

An 8X 60K high-density Agilent array designed with ~150 bp per probe covering the first 6 Mb of chromosome 17p (17pter to 17p13.2) and ~5000 bp per probe covering the remaining chromosome 17 was used. Hybridization controls were gender matched (HapMap individual NA10851 as male control and HapMap individual NA15510 as female control). Scanned array images were processed using Agilent Feature Extraction software (version 10) and extracted files were analyzed using Agilent Genomic Workbench (version 7.0.4.0). In theory, aCGH log2-based intensity ratio between the input sample and control is log2(3/2) = 0.58 for duplications, log2 (4/2) = 1 for triplications, and log2 (5/2) = 1.32 for quadruplications. Array designs and sequence alignment for breakpoint analysis were based on the February 2009 genome build (GRCh37/hg19 assembly).

Breakpoint junction mapping

Primer design and long-rang PCRs for breakpoint junctions mapping were performed as previously described (Gu et al., 2015). Purified PCR products were sequenced by Sanger di-deoxynucleotide sequencing (BCM Sequencing Core, Houston, TX, USA).

ddPCR

ddPCR was performed using the QX200™ AutoDG™ Droplet Digital™ PCR System from Bio-Rad following manufacture's protocols. Briefly, a 20uL mixture was set up for each PCR reaction, containing 10uL of 2x Q200 ddPCR EvaGreen Supermix, 0.25uL of KpnI or *Alu*I

restriction enzyme (NEB, Cat. No. R0142S and R0137S), 0.25uL of each primer (10uM) and 15ng of genomic DNA. Reaction mixture was incubated at 37ºC for an hour for enzymatic digestion, following by automatic droplet generation, PCR reaction and droplet reading. Cycling conditions for PCR are as the following: 5 minutes (mins) at 95ºC, 40 cycles of 30 seconds (sec) at 95ºC / 1 min at 60ºC / 1 min at 72ºC, 5 mins at 4ºC, 5 mins at 90ºC and finally infinite hold at 4ºC. Ramp rate was set for 2ºC per sec for all steps. Data was analyzed using QuantaSoft™ Software from Bio-Rad, and concentrations of positive droplets (number of positive droplets per uL of reaction) were obtained for each PCR reaction. Primer sequences are shown in Supp. Table S1.

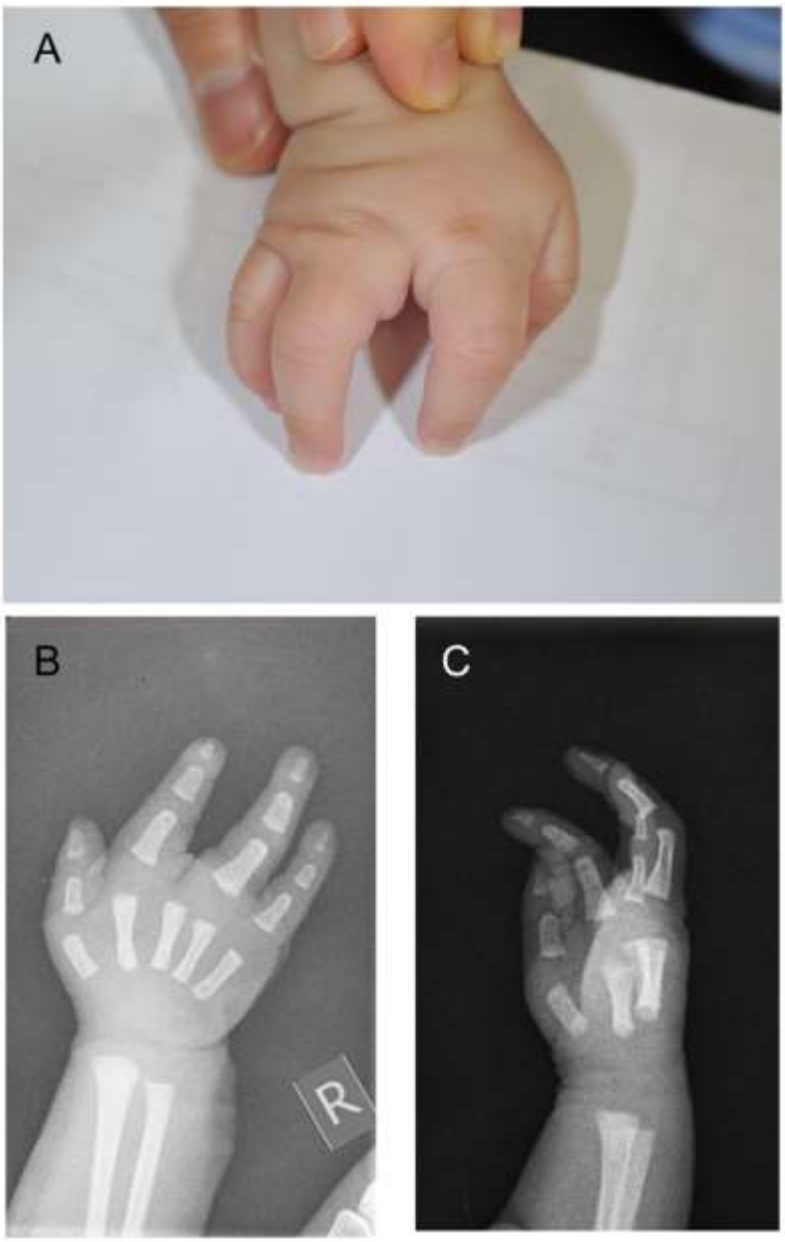

Supp. Figure S1. A). Photograph demonstrates a limb malformation with a median cleft of the right hand and aplasia of the right middle phalange in BAB7221. Posterior /anterior **(B)** and lateral **(C)** radiographs of the right hand demonstrate absent proximal, middle, and distal phalanges of the third digit. All other phalanges and all metacarpals are present and structurally normal.

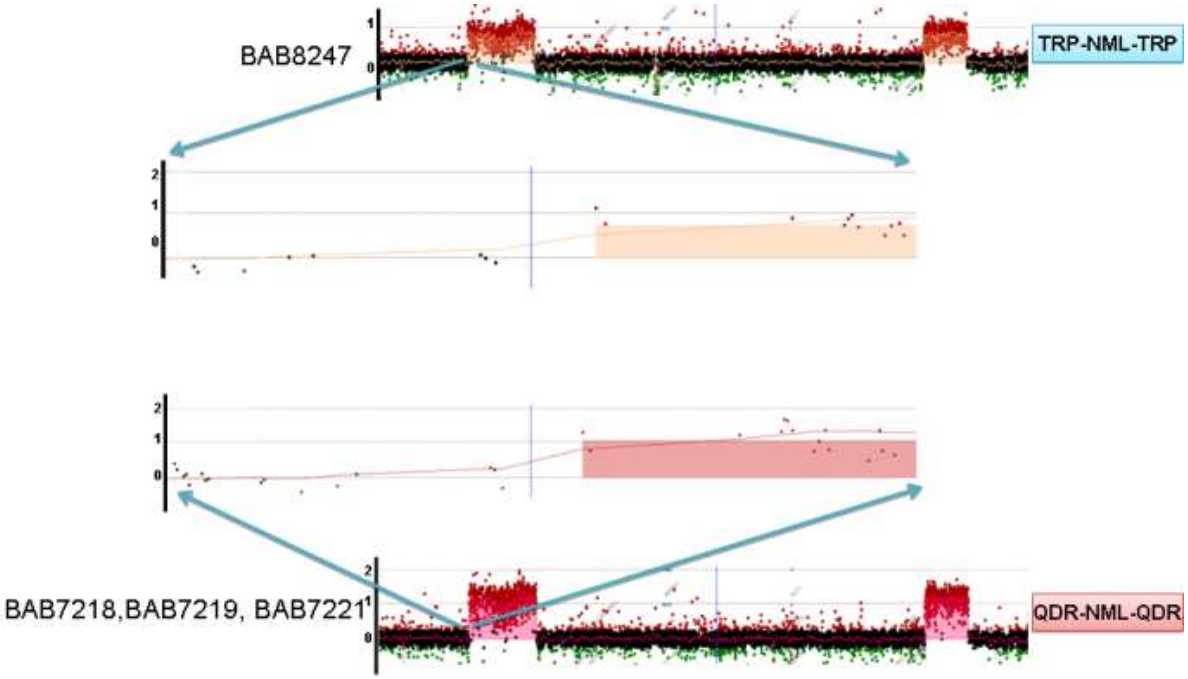

Supp. Figure S2. Enlarged aCGH images of the boundary of the gained region. Quadruplications and triplications detected by high-density aCGH showed sharp edges (direct transition between copy-number gain to copy-number neutral without shoulders) in all four individual tested. Enlarged images of the distal side of the first gain were used for illustration. Array plot of BAB7219 was used for demonstration (lower panel) QDR, quadruplication; NML, normal; TRP, triplication.

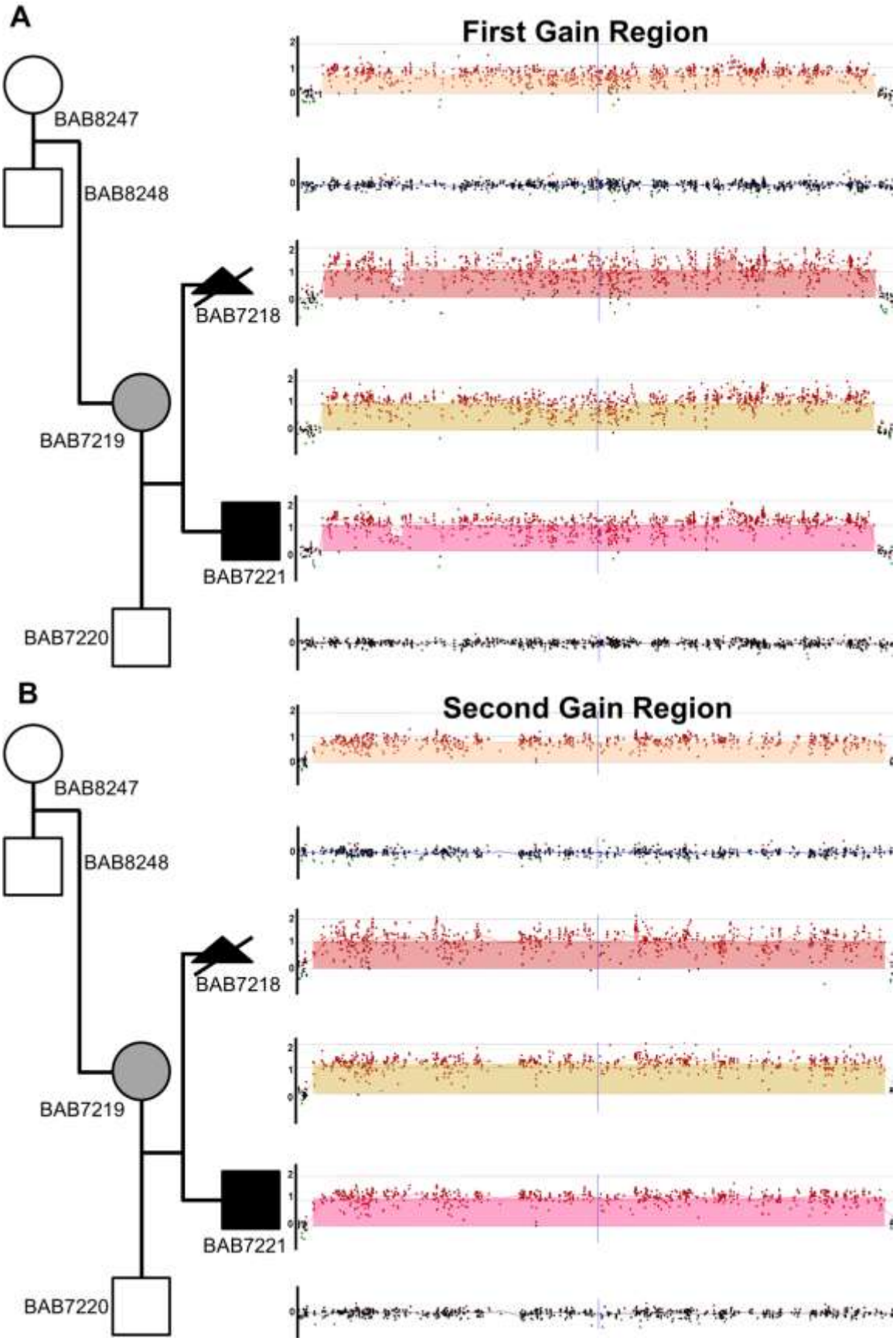
A
First Gain Region
BAB8247
BAB8248
BAB7218
BAB7219
BAB7221
BAB7220
B
Second Gain Region
BAB8247
BAB8248
BAB7218
BAB7219
BAB7221
BAB7220

Supp. Figure S3. Enlarged aCGH images of the two gained regions. Enlarged aCGH images demonstrated higher log2 ratio for both regions in BAB7218, 7219 and 7221 (log2 ratio >1) with two quadruplications in comparison to the log2 ratio in BAB8247 (log2 ratio <1) with two triplications. See also Supp. Table S1.

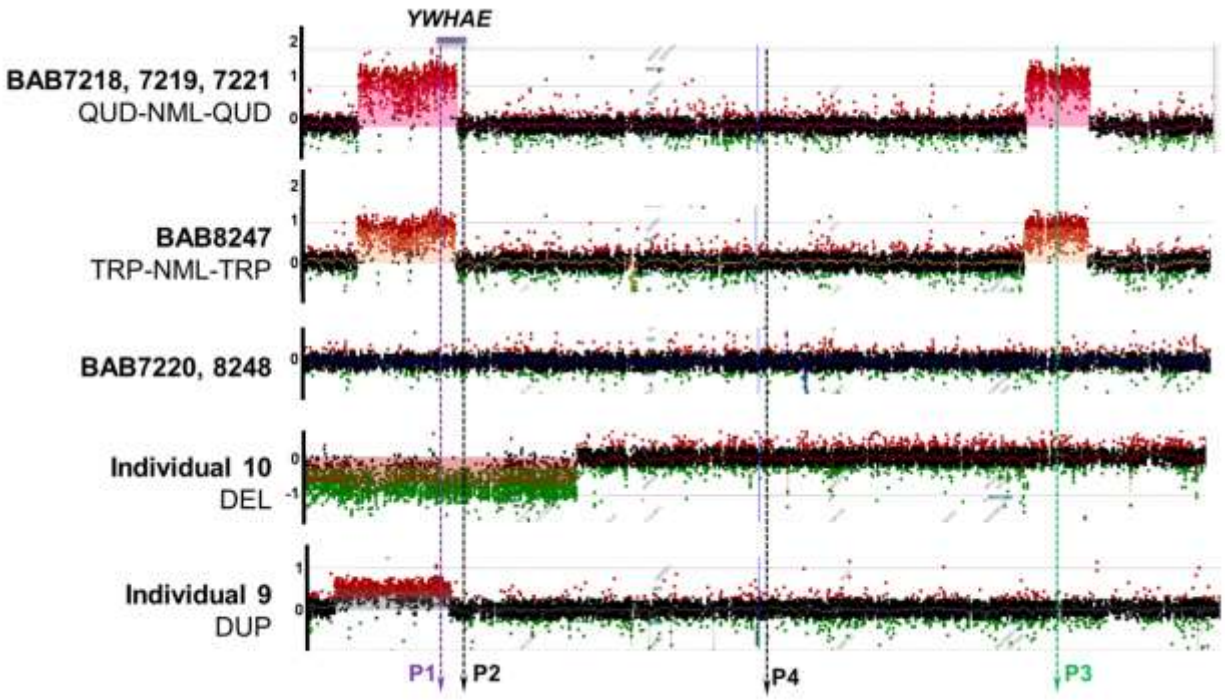

Supp. Figure S4. ddPCR primer pairs. Four pairs of primers, P1, P2, P3 and P4 were used to perform ddPCR; their map positions are demonstrated by different colored vertical lines using representative aCGH images. Note that P1 (purple) and P3 (green) are located in the two regions revealing copy number gains in BAB7218, 7219, 7221 and 8247, respectively, while P2 and P4 (both black) are located in the unaltered copy-number region in between. Both P1 and P2 are designed within the *YWHAE* gene, part of which is quadruplicated / triplicated in the above mentioned four family members. Individual 10 and Individual 9 are previously reported individuals with deletion and duplication at 17p13.3, respectively, and were used for comparison for the ddPCR assays (Gu et al., 2015). Primer sequences are shown in Supp. Table S3. TRP, triplication; NML, normal; QDR, quadruplication; DEL, deletion; DUP, duplication.

.

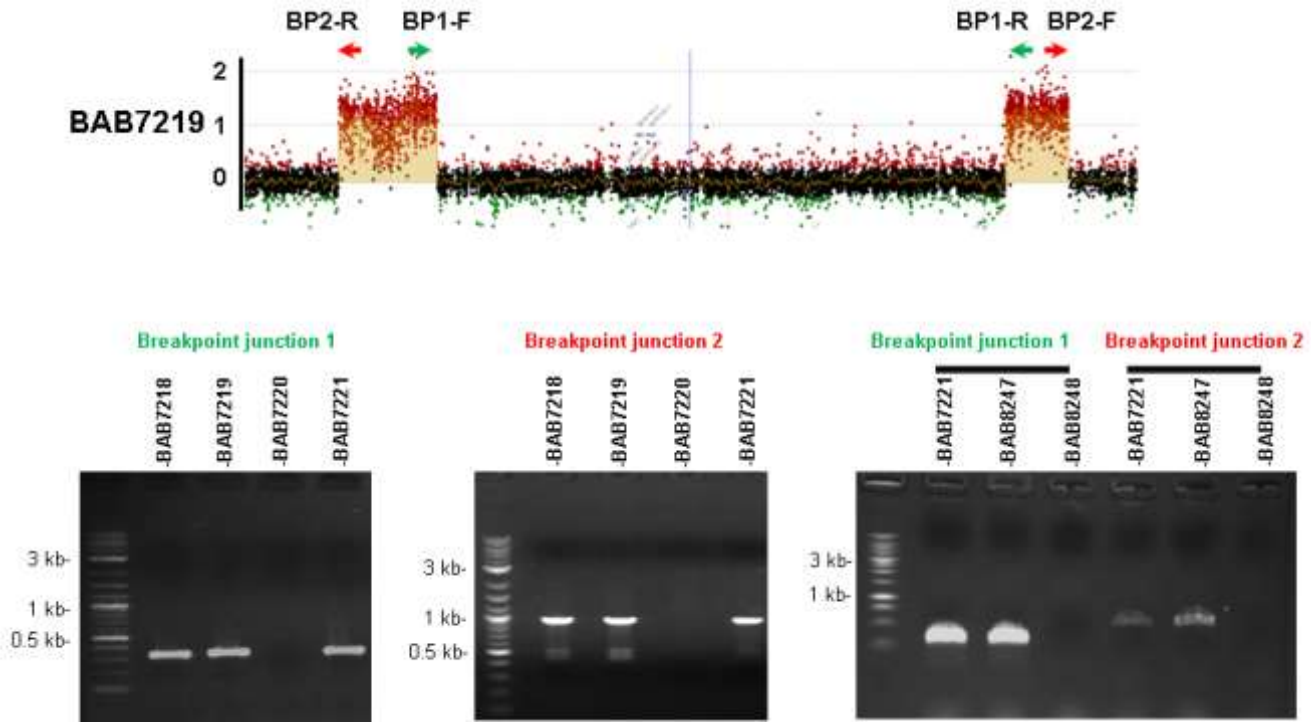

Supp. Figure S5. PCR of the two breakpoint junctions in all the family members. PCR of breakpoint junction 1 used primer pair BP1-F and BP1-R, while PCR of breakpoint junction 2 used primer pair BP2-F and BP2-R (upper panel). Array plot of BAB7219 was shown for demonstration. Both breakpoint junctions were present in BAB7218, BAB7219, BAB7221 and BAB8247 with quadruplications or tripilications, but not in BAB7220 or BAB8248 with no CNV detected. Sequences of the primers are listed in Supp. Table S3.

Supp. Table S1. High Density Array Raw Data, is available as a separate Excel file under the Supporting Information for this article.

Supp. Table S2. ddPCR raw data

Sample	Target	Concentration (droplet/uL)	Copies Per 20uL Well	Poisson ConfMax	Poisson ConfMin	Positives	Negatives	Accepted Droplets
BAB7218	P1	184	3680	190	177	2837	16793	19630
BAB7218	P2	77.9	1558	82.1	73.7	1336	19512	20848
BAB7218	P3	182	3640	188	175	2865	17173	20038
BAB7218	P4	80.8	1616	85.4	76.3	1222	17178	18400
BAB7218	RPPH1	80.4	1608	85.1	75.9	1173	16574	17747
BAB7218	TERT	72.5	1450	76.5	68.5	1256	19758	21014
BAB7219	P1	530	10600	542	517	7040	12373	19413
BAB7219	P2	193	3860	200	186	3134	17561	20695
BAB7219	P3	470	9400	481	458	6571	13391	19962
BAB7219	P4	201	4020	208	194	3016	16171	19187
BAB7219	RPPH1	217	4340	225	209	3130	15461	18591
BAB7219	TERT	182	3640	189	175	2836	16960	19796
BAB7220	P1	182	3640	189	175	2950	17628	20578
BAB7220	P2	171	3420	178	165	2766	17627	20393
BAB7220	P3	198	3960	205	191	3080	16826	19906
BAB7220	P4	183	3660	190	176	2732	16228	18960
BAB7220	RPPH1	181	3620	188	174	2588	15605	18193
BAB7220	TERT	177	3540	185	170	2308	14173	16481
BAB7221	P1	420	8400	431	409	5626	13100	18726
BAB7221	P2	171	3420	177	164	2569	16446	19015
BAB7221	P3	414	8280	425	403	5655	13422	19077
BAB7221	P4	188	3760	194	181	2855	16521	19376
BAB7221	RPPH1	182	3640	189	175	2440	14581	17021
BAB7221	TERT	165	3300	172	157	2059	13714	15773
BAB8247	P1	326	6520	336	317	4480	14025	18505
BAB8247	P2	173	3460	180	166	2709	17103	19812
BAB8247	P3	317	6340	326	307	4343	14059	18402
BAB8247	P4	151	3020	158	145	2308	16806	19114

Sample	Target	Concentration (droplet/uL)	Copies Per 20uL Well	Poisson ConfMax	Poisson ConfMin	Positives	Negatives	Accepted Droplets
BAB8247	RPPH1	149	2980	156	143	1965	14523	16488
BAB8247	TERT	145	2900	151	139	2264	17242	19506
BAB8248	P1	152	3040	158	146	2451	17741	20192
BAB8248	P2	164	3280	171	158	2703	18024	20727
BAB8248	P3	177	3540	183	170	2851	17604	20455
BAB8248	P4	179	3580	186	172	2708	16492	19200
BAB8248	RPPH1	165	3300	172	159	2531	16776	19307
BAB8248	TERT	154	3080	161	147	1925	13736	15661
Individual 10	P1	75.7	1514	79.9	71.6	1279	19237	20516
Individual 10	P2	71.7	1434	75.8	67.7	1219	19392	20611
Individual 10	P3	155	3100	161	149	2563	18206	20769
Individual 10	P4	158	3160	164	152	2384	16582	18966
Individual 10	RPPH1	158	3160	164	152	2377	16535	18912
Individual 10	TERT	144	2880	150	137	1832	14111	15943
Individual 9	P1	224	4480	231	216	3630	17328	20958
Individual 9	P2	145	2900	151	139	2374	18119	20493
Individual 9	P3	170	3400	177	164	2662	17076	19738
Individual 9	P4	167	3340	174	161	2418	15837	18255
Individual 9	RPPH1	161	3220	167	154	2371	16173	18544
Individual 9	TERT	162	3240	169	155	2090	14153	16243
N/A 10851	P1	174	3480	181	168	2747	17227	19974

Sample	Target	Concentration (droplet/uL)	Copies Per 20uL Well	Poisson ConfMax	Poisson ConfMin	Positives	Negatives	Accepted Droplets
N/A 10851	P2	187	3740	194	180	2887	16733	19620
N/A 10851	P3	170	3400	177	164	2718	17470	20188
N/A 10851	P4	187	3740	193	180	2879	16753	19632
N/A 10851	RPPH1	186	3720	193	179	2819	16438	19257
N/A 10851	TERT	177	3540	184	170	2815	17341	20156
BAB7218	Jct_ctrl	51.2	1024	54.7	47.7	814	18307	19121
BAB7218	Jct1	73.9	1478	78.2	69.6	1156	17834	18990
BAB7218	Jct2	73.6	1472	77.8	69.3	1155	17901	19056
BAB7219	Jct_ctrl	121	2420	127	116	1822	16808	18630
BAB7219	Jct1	174	3480	181	166	2239	14078	16317
BAB7219	Jct2	170	3400	178	163	2041	13113	15154
BAB7221	Jct_ctrl	127	2540	132	122	2105	18476	20581
BAB7221	Jct1	159	3180	166	153	2543	17517	20060
BAB7221	Jct2	175	3500	181	168	2731	17054	19785
BAB8247	Jct_ctrl	109	2180	115	104	1661	17049	18710
BAB8247	Jct1	98	1960	103	93.1	1510	17382	18892
BAB8247	Jct2	95.1	1902	99.8	90.4	1575	18712	20287

Supp. Table S3. Primer sequences

Name	Sequence (5' - 3')
P1-F	CGCTTGTAAGCAACCATGAGATGTG
P1-R	TGCCTACTGTGGTTGGATGTGATGT
P2-F	CCGCACTCAATAAAGGAATGGACAC
P2-R	CTTGGGGCATAAGGTAGGGACTCAG
P3-F	GACTCCATTTCTGTGGGTGTTGGTT
P3-R	GTTGCCCCTGGATTAACCCTCTTTT
P4-F	TGATGTCAAAACTGAACTTGTGCTGGT
P4-R	CAGGAACCGCAATCAGATCTCTAAGG
RPPH1-F	AATGGGCGGAGGAGAGTAGTCTGAAT
RPPH1-R	CGAAGTGAGTTCAATGGCTGAGGTG
TERT-F	GCACACCTTTGGTCACTCCAAATTC
TERT-R	CCACATAGGAATAGTCCATCCCCAGAT
Jct_ctrl-F	TTGTTCTTCTCTGCGTCCTGCTTTC
Jct_ctrl-R	CCATGGTCACCCTGTGGATCTACTC
Jct1-F	TGCTGCACAATCGTAAGTTGCTAGT
Jct1-R	AACCCTGTTTTCCTCACATGCTGTC
Jct2-F	GTAGCTCAGCATGTTCACTGGAGCA
Jct2-R	CGCATCAGTGTCTAACCCATCACAG
BP1-F	AAAGATTTATGCTCGACCGGG
BP1-R	GCTTGGCCCCATTGTGATTT
BP2-F	GTGCCTGGCAACATGTATTT
BP2-R	CACACCCAGCTAAttttgtttctct

Supp. Reference

Gu, S., Yuan, B., Campbell, I.M., Beck, C.R., Carvalho, C.M., Nagamani, S.C., Erez, A., Patel, A., Bacino, C.A., Shaw, C.A., Stankiewicz, P., Cheung, S.W., *et al.* (2015). Alu-mediated diverse and complex pathogenic copy-number variants within human chromosome 17 at p13.3. Hum Mol Genet *24*, 4061-4077.